Available online at www.sciencedirect.com
ScienceDirect
Journal of Catalysis 254 (2008) 101–109
JOURNAL OF CATALYSIS
www.elsevier.com/locate/jcat

Synthesis methodology, stability, acidity, and catalytic behavior of the 18 × 10 member ring pores ITQ-33 zeolite

Manuel Moliner, María J. Díaz-Cabañas, Vicente Fornés, Cristina Martínez, Avelino Corma *

Instituto de Tecnología Química, UPV-CSIC, Universidad Politécnica de Valencia, Avda. de los Naranjos s/n, 46022 Valencia, Spain

Received 7 September 2007; revised 30 November 2007; accepted 2 December 2007

Abstract

We used a flexible organic structure-directing agent (OSDA) and high-throughput (HT) synthesis techniques to explore a large composition region. A zeolite with the largest pores reported to date (ITQ-33) was found under very unusual synthesis conditions, together with other known structures. A second HT experimental design allowed, finally synthesizing pure ITQ-33. We studied the thermal and hydrothermal stability and acid properties of the zeolite. We investigated the role of pore diameter on zeolite acid strength by comparing the 18-ring pore (ITQ-33) with a 12-MR pore (ITQ-17) zeolite with the same framework composition. Finally, we compared the catalytic properties of ITQ-33 for reactant molecules of different sizes with those of 12-MR (Beta) and 14-MR (UTD-1) zeolites.

Keywords: Extra-large pore zeolite; High-throughput synthesis; Experimental design; Acid strength; Benzene alkylation; Cracking

1. Introduction

Zeolites are microporous crystalline materials with ever-increasing applications for gas separation, selective catalysis, electronic, and biomedical uses [1–4]. The great advantage of zeolites is their thermal and chemical stability along with the ability to vary pore dimensions and topology, as well as framework composition, by controlling synthesis conditions. But despite significant efforts to rationalize the synthesis of zeolites, there remains poor knowledge on the nature of the nucleation species and on how to predict the characteristics of material that will be obtained under a given set of synthesis conditions [5–8].

Nevertheless, the synthesis of new materials has been advanced through the introduction of new concepts regarding the effects of organic and inorganic structure-directing agents [9–14]. In reference to this, the concept that rigid organic-structure directing agents (OSDA) can be more selective toward a particular structure was first presented a decade ago [15]. This concept has been the key to creating numerous new structures [16–19]. More flexible OSDAs are in general less selective, in many cases giving a mixture of phases. However, the flexible organics may have the advantage of adopting a large number of conformations, making them interesting for synthesizing new structures. Using hexamethonium has made it possible to produce new phases such as IM-10, EU-1, ITQ-13, ITQ-22, ITQ-24 [20–25], and, recently, ITQ-33 [26], depending on such synthesis variables as crystallization temperature, time and composition of the starting gel.

A few years ago, we decided to move from rigid to more flexible OSDAs. The combination of OSDA with a higher number of degrees of freedom and the use of in-house-developed high-throughput (HT) synthesis techniques, HT characterization tools, and data management [27] gives us the ability to explore these OSDAs in a larger experimental space and also direct the synthesis toward a particular structure in a mixture of phases by means of the appropriate experimental design [28].

In this paper we discuss in detail how this methodology has allowed us to first obtain a mixture of phases in which the ITQ-33 zeolite [26], with a unique topology formed by extra-large 18-MR pores crossing 10-MR pores, is present, and then to direct the synthesis selectively toward the new zeolite until

* Corresponding author. Fax: +34 96 3877809.
E-mail address: acorma@itq.upv.es (A. Corma).

0021-9517/$ – see front matter © 2007 Published by Elsevier Inc.
doi:10.1016/j.jcat.2007.12.003

achieving the pure phase. In the second part of the paper, we report on the acid properties of the material and the affect of pore diameter on acid strength, as well as the stability of ITQ-33 under different atmospheres and treatments, along with some catalytic properties.

2. Experimental

2.1. Materials and synthesis

Synthesis gels were prepared using a robotic system [29] composed of a robotic arm for vial handling and solid weighing, a stirring station for gel homogenization and evaporation, and a liquid dosing station equipped with pumps and an analytical balance. In the typical robotic synthesis procedure for ITQ-33, boric acid (99.5%, Aldrich) or alumina (74.6%, Condea) and germanium oxide (99%, Aldrich) are dissolved in hexamethonium bromide (pure, Fluka) and hexamethonium hydroxide solutions. Then colloidal silica (Ludox AS-40, Aldrich) is added, followed by NH_4F (98%, Aldrich) if necessary.

The synthesis gel was introduced in vials (3 ml), which were inserted into a 15-well multisample autoclave. Crystallization was carried out at 443 K under static conditions. After filtration, washing, and drying, the samples were characterized by XRD using a multisample Philips X'Pert diffractometer using CuK_α radiation. The composition of a typical synthesis gel in fluoride media to obtain ITQ-33 was as follows: $0.67SiO_2$:$0.33GeO_2$:$0.050Al_2O_3$:$0.15Hex(OH)_2$:$0.10Hex(Br)_2$:$0.30HF$:$1.5H_2O$, with synthesis conditions of 443 K for 5 h under static conditions.

2.2. Acidity measurements

Infrared spectra were measured with a Nicolet 710 FT IR spectrometer. Pyridine adsorption–desorption experiments were carried out on self-supported wafers (10 mg cm^{-1}) of original samples previously activated at 673 K and 10^{-2} Pa for 2 h. After wafer activation, the base spectrum was recorded, and pyridine vapor (6.5×10^2 Pa) was admitted into the vacuum IR cell and adsorbed onto the zeolite. Desorption of pyridine was performed in vacuum over three consecutive 1-h periods of heating at 423, 523, and 623 K, each followed by an IR measurement at room temperature. All of the spectra were scaled according to the sample weight. Adsorption of ditertbutyl pyridine (DTBP) was performed in the same way, but with desorption done only at 423 K.

2.3. Catalytic experiments

1,3-Diisopropylbenzene (DIPB) and 1,3,5-triisopropylbenzene (TIPB) were cracked in an automated microactivity test unit at 773 K, at catalyst-to-oil ratios ranging from 0.3 to 0.8 g/g, using 0.2 g of catalyst. Cyclic experiments involved the following steps: (a) stripping of the catalyst with N_2 for 20 min, followed by reaction during 60 s time on stream (TOS), (b) stripping with N_2 at reaction temperature (20 min, 30 ml/min), and (c) regenerating the catalyst at 793 K for 3 h with an air flow of 80 ml/min. The gaseous and liquid fractions of the product were analyzed by gas chromatography. The solid products (coke) deposited on the catalyst during the reaction were quantified by the CO_2 produced during regeneration, measured with an online IR detector. Only experiments with mass balances >95% were considered. Kinetic rate constants were obtained by fitting the conversion data obtained at different contact times to a first-order kinetic rate equation.

Alkylation of benzene with propylene was carried out on the acid zeolites, which were pelletized, crushed, and sieved at 0.25–0.42 mm diameter. The reaction was performed in an automated high-pressure stainless steel reactor at 398 K, 3.5 MPa, a benzene/propylene molar ratio of 3.5, and a space velocity (WHSV) ranging from 12 to 24 h^{-1} referred to the olefin. Samples were analyzed by online gas chromatography at different TOS by means of a 30-m 5% phenyl–95% dimethylpolysiloxane column, with an internal diameter of 0.25 mm and 1 μm of phase film thickness.

3. Results and discussion

An initial factorial design (3×4^3) was performed for synthesis in OH^- media for exploring different molar gel compositions. This experimental design considers the following four molar ratios (level): Si/Ge(4) of 2–30, B/(Si + Ge)(4) of 0–0.05, OH/(Si + Ge)(3) of 0.1–0.5, and H_2O/(Si + Ge)(4) of 5–30. The total number of samples synthesized considering this design was 192.

Fig. 1 shows the phase diagram obtained with this first screening after 14 days of crystallization time. The different competing phases as a function of the starting gel composition can be observed. Despite the nonlinearity of the system, the range of compositions in which each specific phase is formed is clearly defined, although there are some narrow ranges in which two or more phases are competing. Five different known materials (ITQ-22 [24], ITQ-24 [25], EU-1 [21], SSZ-31 [30], and a layered phase) were obtained in the range of gel compositions explored. Moreover, an unknown crystalline material was formed along with ITQ-24 in a specific area of the phase diagram. The experimental conditions for the synthesis of this unknown material are extremely unusual, owing to the low concentration of the silica-mobilizing agent OH^- (OH^-/(Si + Ge) = 0.1) and the high concentration of the gel (H_2O/(Si + Ge) = 5). The synthesis occurred in the presence of trivalent atoms ((Si + Ge)/B = 20 or 50) and germanium (Si/Ge = 2).

Along with this new material, the following known crystalline phases were obtained in the synthesis region explored:

- ITQ-24, which is obtained due to its high content of Ge and trivalent atoms, also incorporating high OSDA loadings. Previously, ITQ-24 zeolite was obtained in OH^- media with a Si/Ge ratio of 5 and from diluted gels (H_2O/T^{IV} = 30) [25]. However, in our present study, using HT synthesis, this zeolite also was formed with a Si/Ge ratio of 15, with trivalent atoms and from concentrated gels, as shown in Fig. 1.

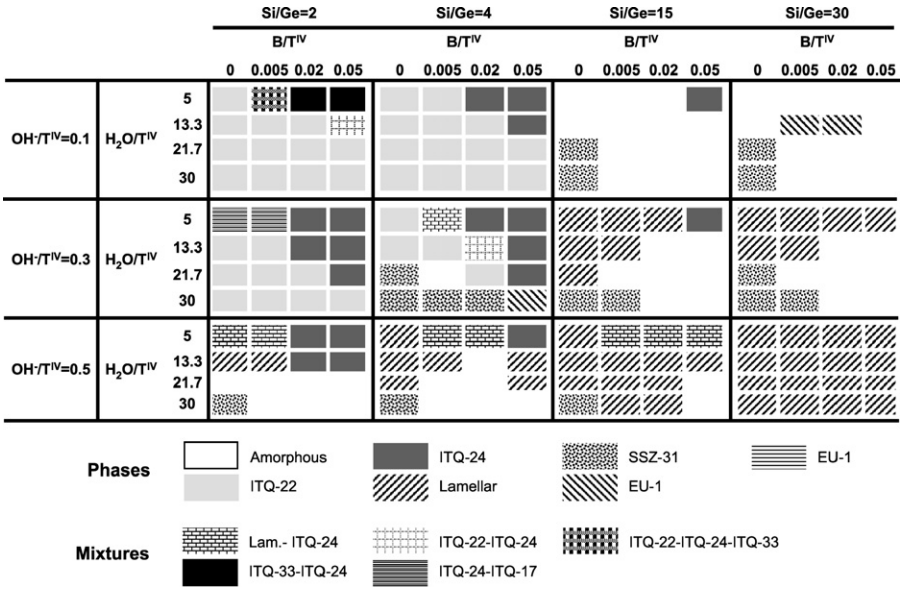

Fig. 1. Phase diagram obtained for the initial experimental design in OH^- media. The synthesis conditions were $T = 448$ K and $t = 14$ days, ratio $SDA/T^{IV} = 0.25$.

- ITQ-22, which incorporates less OSDA than ITQ-24 but is more favored than ITQ-24 when lowering the Si/Ge ratio and decreasing the boron concentration.
- EU-1, which appears at higher Si/Ge ratios and from less concentrated synthesis gels than ITQ-24, but with a high boron content.
- SSZ-31, which is obtained with very high T^{IV}/B ratio compositions and diluted systems. The synthesis of this zeolite was never reported before with hexamethonium as OSDA. Most OSDAs reported for the synthesis of SSZ-31 have been bulkier and more hydrophobic cations. We also found that SSZ-31 can crystallize with large amounts of Ge in the synthesis gel.
- A layered material that is formed for high OH^- concentration and starts to dissolve when any zeolitic crystal begins to grow, and appears to be a source of T atoms for the synthesis of zeolites. The layered phase is thermally unstable, and the structure collapses when calcined at 823 K.

The new crystalline phase present in the mixture was named ITQ-33. The X-ray diffractogram (XRD) shows a first peak appearing at a very low 2θ values ($2\theta = 5°$). Although there is no general rule correlating low 2θ angle with large pore diameter, this correlation is frequently observed. Therefore, we considered in a first approximation that the ITQ-33 should have large or extra-large pores.

To design the second experimental generation directed to produce pure ITQ-33, we analyzed the results from the first set of synthesis experiments by means of statistical tools, such as Pareto analysis, using the framework density of each zeolite (measured as T atoms per 1000 $Å^3$) as output. This method allowed quantification of the hypothetical weight of each variable in the final result. The chart produced is a frequency histogram that arranges the parameters according to their influence, with the most important on top. In the chart, the length of each bar is the estimated effect divided by its standard error, which is

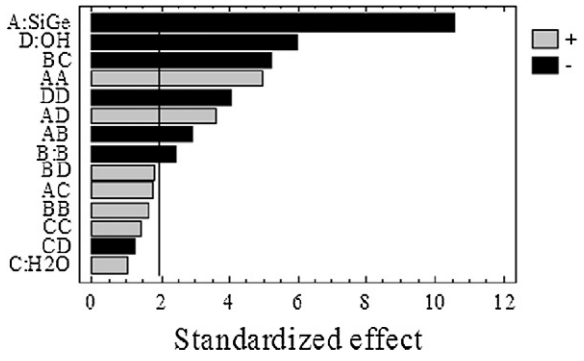

Fig. 2. Pareto analysis showing the relative influence of each variable over the different formed phases.

equivalent to computing a t-statistic for each effect. Bars extending the vertical line on the plot correspond to effects that are statistically significant at a 95% confidence level. These statistical approaches, used to interpret the results, allow quantification of the hypothetical weight of the factors influencing the growth of the desired material.

The results presented in Fig. 2 show that variables with a stronger influence on the synthesis of ITQ-33 include Si/Ge, $OH^-/(Si + Ge)$, and the combination of $B/(Si + Ge)$ and $H_2O/(Si + Ge)$. Based on this finding, we carried out a second set of 18 synthesis experiments. The results, shown in Fig. 3, demonstrate that by following the indications from the Pareto analysis, ITQ-33 can be obtained as pure crystalline phase with a very small amount of amorphous material.

Because all of the zeolites obtained with high Ge content contain double four ring (D4R) units in the structure, it is reasonable to suppose that they are present in the ITQ-33 structure as well. It is well known that F^- also stabilizes D4R [31]; consequently, we carried out a third set of synthesis experiments using F^- as mineralizer to favor the formation of ITQ-33. The factorial experiment was a $3^2 \times 4$ design, which gave a total of 36 experiments. The molar ratios (level) were Si/Ge(4) rang-

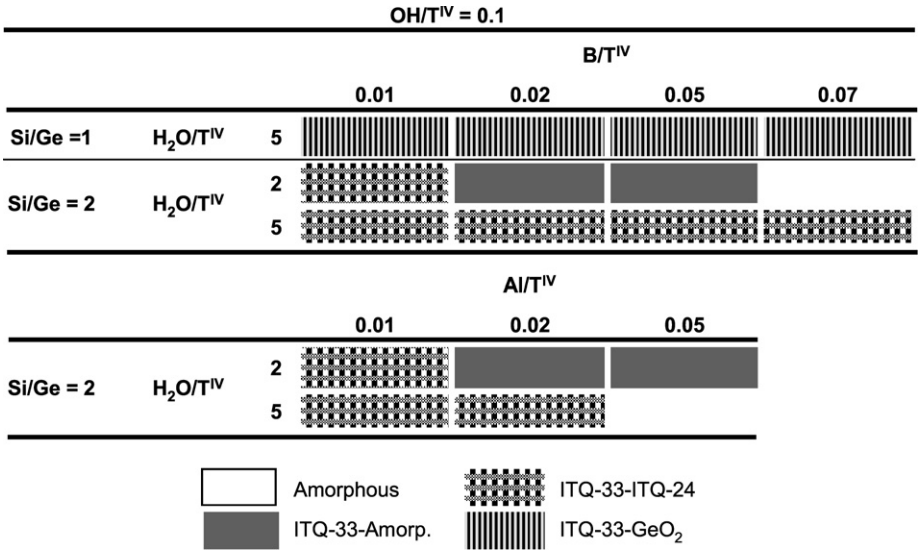

Fig. 3. Phase diagram for the second experimental design in OH^- media. The synthesis conditions were $T = 448$ K and $t = 14$ days, ratio $SDA/T^{IV} = 0.25$.

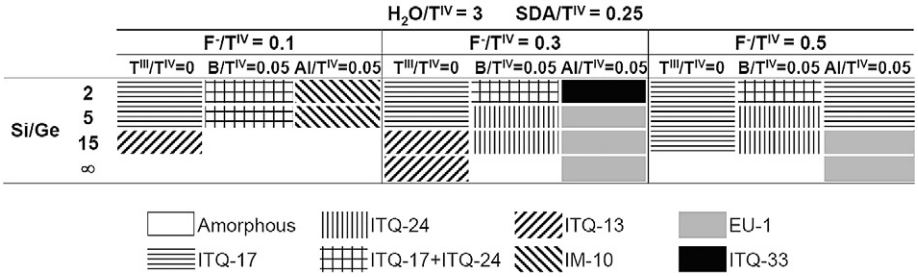

Fig. 4. Phase diagram obtained in F^- media, getting the crystalline ITQ-33 in narrow conditions. The synthesis conditions were $T = 448$ K and $t = 14$ days, ratio $SDA/T^{IV} = 0.25$.

ing from 2 to ∞; $T^{III}/T^{IV}(3) = 0$, 0.05(Al), 0.05(B); $F^-/T^{IV}(3)$ from 0.1 to 0.5.

The phase diagram thus obtained is shown in Fig. 4. The phases obtained were ITQ-13, ITQ-17, ITQ-24, IM-10, EU-1, and pure ITQ-33, with a composition $0.67SiO_2{:}0.33GeO_2{:}0.050Al_2O_3{:}0.15Hex(OH)_2{:}0.10Hex(Br)_2{:}0.30HF{:}1.5H_2O$. We studied the stability and acidity of the pure ITQ-33.

3.1. ITQ-33 stability

The crystalline ITQ-33 was calcined at 823 K under He/O_2 flow in an Anton Paar XRK-900 reaction chamber attached to a Philips X'Pert diffractometer. After cooling at room temperature, the XRD pattern was obtained; it showed that the sample was highly crystalline after calcination (see Fig. 5).

A sample of ITQ-33 with Si/Ge = 2 and $T^{IV}/Al = 20$ containing the OSDA within the pores was left in contact with moisture at room temperature for 6 months, after which time no changes in the crystallinity of the sample could be detected. A pelletized sample of ITQ-33 (0.42–0.60 mm diameter, pressure = 4 Tm/cm^2) was calcined at 813 K and then exposed to ambient conditions at room temperature. Then the micropore volume was measured after 7, 14, and 30 days; the results, given in Table 1, show that the calcined ITQ-33 retained most of the micropore volume after 14 days, but lost 50% of the volume after 30 days of exposure to moisture at room temperature.

From the foregoing results, we can conclude that ITQ-33, with the template inside the pores, can be stored for at least 6 months with no damage to the structure. ITQ-33 is stable to calcination and, in the pelletized form, slowly degrades with time if exposed to humidity at room temperature after calcination. This is likely due to the presence of large amounts of Ge in the structure that will coordinate H_2O when the zeolite is exposed to H_2O at room temperature, changing the coordination from 4 to 6. In contrast, a calcined sample in contact with air (80% humidity) exposed to ambient conditions at temperatures $\geqslant$623 K sustains no structural damage.

3.2. Acidity characterization and acid site accessibility

When a self-supporting wafer of Al-ITQ-33 ($T^{IV}/T^{III} = 20$) was calcined in the IR cell at 673 K and 10^{-2} Pa, all OSDA was removed, and the IR spectra in the OH stretching region showed the presence of three bands at 3740, 3675, and 3608 cm^{-1} (Fig. 6a) associated with the presence of silanols, germanols, and bridging hydroxyl groups, respectively [32]. After pyridine was adsorbed at room temperature and then desorbed at 423 K in vacuum to remove the physically adsorbed pyridine (see Fig. 6b), some changes in the IR spectrum were visible.

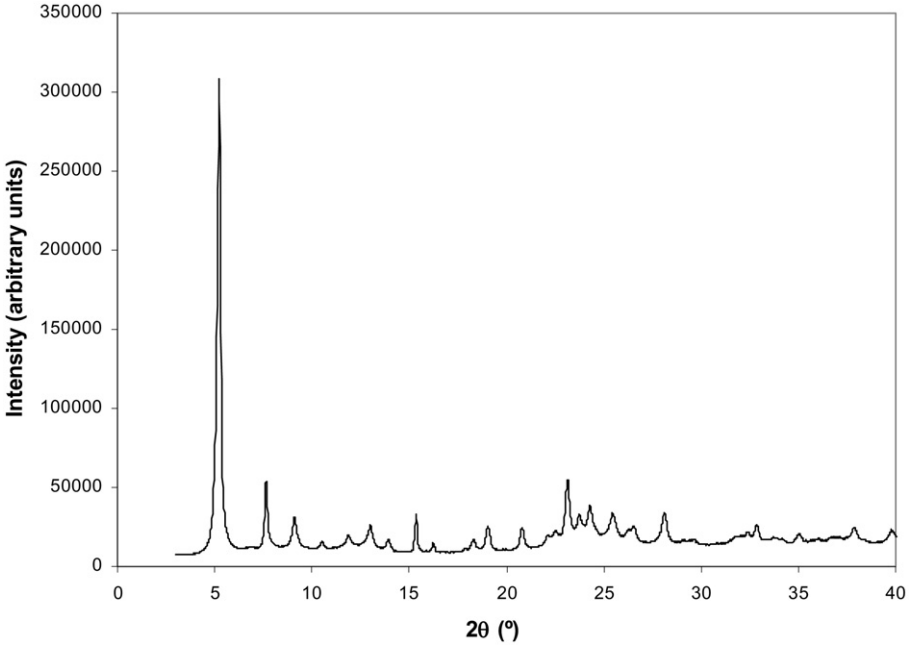

Fig. 5. XRD diffraction pattern for the calcined ITQ-33.

Table 1
Values of BET surface area, micropore area, and micropore volume for the pelletized ITQ-33 at different times in humidity conditions

Time (days)	BET surface area (m^2/g)	Micropore area (m^2/g)	Micropore volume (cm^3/g)
0	655.2	578.9	0.275
7	625.4	565.4	0.270
15	621.4	535.4	0.259
30	230.5	163.1	0.085

The intensity of the bands associated to silanol and germanol groups (3740 and 3675 cm^{-1}) increased, indicating that the introduction of pyridine and subsequent desorption caused some hydrolysis of Si–O–Ge bonds. The adsorption of pyridine also caused the disappearance of the band associated with bridging OH groups, due to protonation of the pyridine. Indeed, the IR spectrum of the pyridine adsorbed after evacuation at 423 K clearly showed the presence of bands at 1545 and 1638 cm^{-1}, which are associated with protonated pyridine (see Fig. 6c). The same spectrum also shows IR bands at 1452, 1610, and 1622 cm^{-1} that can be associated with pyridine coordinated

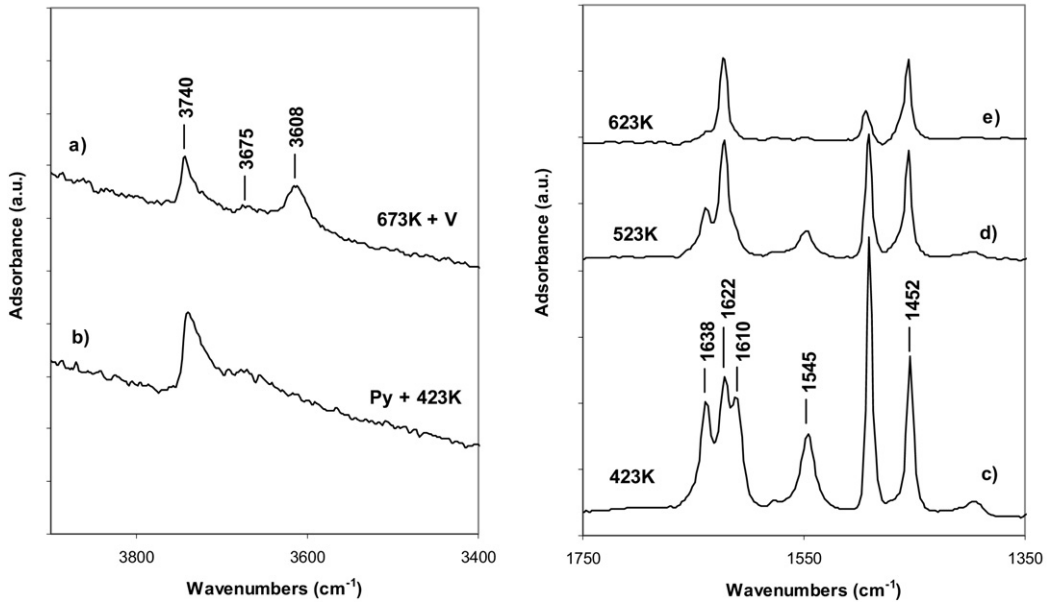

Fig. 6. Acid properties of Al-ITQ-33 zeolite measured by pyridine adsorption/stepwise desorption at different temperatures. On the left is plotted the stretching hydroxyl region, where (a) is the IR spectrum upon thermal treatment at 673 K under vacuum, and (b) is after adsorbing pyridine followed by desorption at 423 K. On the right is shown the stretching C–C region of the adsorbed pyridine upon desorption at (c) 423, (d) 523, and (e) 623 K.

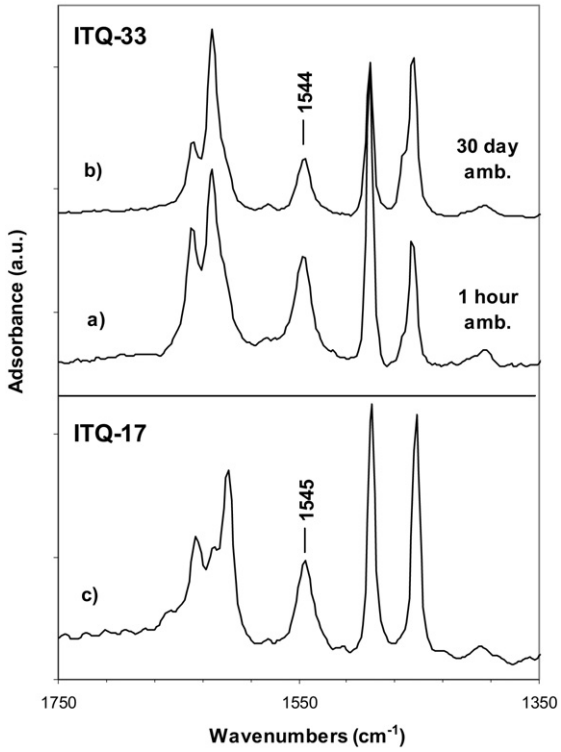

Fig. 7. IR spectrum in the stretching C–C region of the adsorbed pyridine upon desorption at 423 K, (a) for ITQ-33 after exposure to humidity for one our, (b) for ITQ-33 after exposure to humidity for 30 days, (c) for the Al-ITQ-17 (Si/Ge = 2).

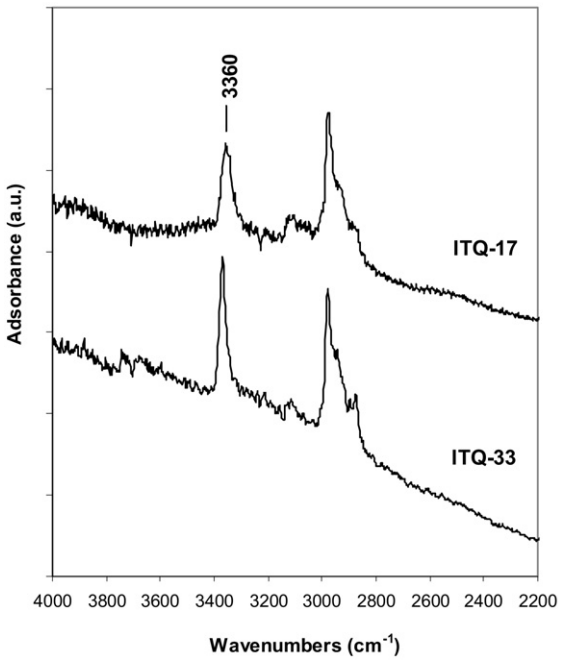

Fig. 8. IR spectrum in the stretching hydroxyl region for the ITQ-17 and ITQ-33 (Si/Ge = 2; $T^{IV}/T^{III} = 20$) after adsorbing DTBPy followed by desorption at 423 K.

to Lewis acid sites. More specifically, the band at 1622 cm^{-1} should correspond to pyridine coordinated to extra-framework aluminum as a Lewis acid, and the band at 1610 cm^{-1}, which we detected exclusively in Ge-containing zeolites, indicates sites of weaker Lewis acidity and should be associated with pyridine coordinated to Ge [33]. Notice that after evacuation at 523 K (Fig. 6d), pyridine associated with Brönsted (bridging hydroxyls) and Lewis acids remained, except in those associated with Ge, which as stated earlier, are weaker Lewis acids. The relative intensity of the 1545-cm^{-1} pyridine band after desorption at 423 and 523 K (Figs. 6c and 6d) clearly shows that an important fraction of the Brönsted acid sites cannot retain the pyridine adsorbed at the higher temperatures, indicating that ITQ-33 is of medium to strong Brönsted acidity. Indeed, at a pyridine desorption temperature of 623 K, only a very small amount of pyridine remained protonated on strong acid sites.

We also studied the influence of zeolite stability on acidity by performing the following "in situ" IR experiments. A self-supporting wafer of ITQ-33 was calcined at 673 K and 10^{-2} Pa for 20 h, after which the IR spectra was recorded. Then the IR cell was opened, and air (85% relative humidity) was admitted at room temperature for 1 h. After calcining again at 673 K in vacuum for 20 h, pyridine was adsorbed at room temperature and desorbed at 423 K, after which the IR spectrum was again recorded. Comparing the results, given in Fig. 7a, with those of Fig. 6c shows that the exposure to humidity for 1 h had no effect on the intensity of the pyridinium ion band at 1545 cm^{-1}. This means that the sample retained the Brönsted acidity, in agreement with the previous findings on the effect of treatment on micropore volume. However, when the exposure to humid air was prolonged for 30 days, the resulting IR spectrum (Fig. 7b) shows a loss of approximately 50% of the Brönsted acidity, in excellent agreement with previous data on micropore volume and stability.

Consequently, from the IR characterization results, we can conclude that the zeolite ITQ-33 has medium to strong Brönsted acidity and that in pelletized (wafer) form, it is stable after calcination and exposure to humidity for a certain period, in good agreement with the micropore volume retention after the treatments.

An advantage of ITQ-33 with respect to other zeolites is its larger pore diameter. We have found here that all Brönsted acid sites are accessible to a larger base, such as di-tertbutyl-pyridine (DTBPy) (see Fig. 8), because after adsorption of DTBPy, all of the bridging hydroxyl groups (3610 cm^{-1}) disappeared, while a band at 3360 cm^{-1} associated with protonated DTBPy was clearly visible.

3.3. Comparison of the acidities of extra-large-pore (ITQ-33) and large-pore (ITQ-17) zeolites

It is commonly believed that the acid strength of the zeolites should increase with decreasing pore diameter. This effect is explained based on the differences in the distribution and density in the electric field gradients within the zeolites with different pore diameters as well as the differences in Van der Waals adsorption effects [34,35]. If this were so, then we would have to conclude that the larger the pore diameter, the weaker the acid strength. But if we take into account that the proton transfer (especially when reacting with a base) occurs in a highly localized

mode, then differences in acidity probably are more closely related to T–OH–T′ constraints in the angles (and thus with the tendency to donate the proton to release that constraint in the structure) than to pore diameter.

To investigate these effects, we prepared two zeolites, one with 10-MR pores and another with 12-MR pores, with the same composition as ITQ-33. By doing so, we had zeolites with pore diameters of ≅0.55, 0.70, and 1.2 nm. Unfortunately, we were unable to synthesize any 10-MR pore zeolite sample with the same Si/Ge and T^{III}/T^{IV} ratio as ITQ-33, but we succeed in preparing a 12-MR pore zeolite (ITQ-17) with the same composition as ITQ-33.

Following the same methodology as before, pyridine was adsorbed on a sample of ITQ-17 (BEC structure) with a Si/Ge = 2 and $T^{IV}/T^{III} = 20$. The results (Fig. 7c) show that the pyridinium ion band was of slightly lower intensity for ITQ-33 (Fig. 7a) than for ITQ-17 (Fig. 7c). Moreover, the intensity of the band was relatively similar for the two samples when desorbing at 523 K, indicating that not only the total Brönsted acidity, but also the acid strength should be similar for the two samples. Therefore, we must conclude that we cannot detect very important differences in acid strength, at least when comparing the two zeolites reported here, although the 12-MR seems slightly more acidic. In other words, and if we try to reconciliate the results obtained here with those reported by Eder et al. comparing ZSM-5 and USY zeolites [35], we would conclude that the influence of pore diameter on acidity should be less important when going from large-pore to extra–large-pore zeolites.

However, we have observed differences in acid site accessibility among the two samples when using the bulkier DTBPy amine as a probe molecule. The results, presented in Fig. 8, clearly show that the intensity of the 3360 cm^{-1} band associated with protonated DTBPy [36] was significantly higher for ITQ-33 than for ITQ-17. In other words, although the smaller-sized amine (pyridine), which can easily diffuse in 12-MR pore zeolites, gave the same number of Brönsted acids (same amount of protonated pyridine) for ITQ-17 and ITQ-33, DTBPy, with constraints to diffuse inside the 12-MR pore zeolites, gave more Brönsted acid sites in ITQ-33 than in ITQ-17. This finding again demonstrates the attraction of the extra-large-pore zeolite from the standpoint of accessibility of its acid sites to large reactant molecules.

To demonstrate the suitability of zeolite ITQ-33 as a solid acid catalyst, we expanded the preliminary catalytic results presented in previous work [26].

3.4. Catalytic experiments

The catalytic cracking process (FCC), currently based on zeolite Y, converts bulky hydrocarbons into more valuable fractions, such as light olefins and liquid fuels. Finding of new zeolites with more accessible structures poses a challenge. Preliminary results [26] have shown that ITQ-33 has activity for conversion of a vacuum gasoil comparable to that of a USY zeolite and also is highly selective to diesel and propylene. These properties are enhanced by combining the ITQ-33 with a medium-pore zeolite. On the other hand, catalytic cracking of pure compounds with different kinetic diameters has been proven to be a useful tool not only for determining the intrinsic catalytic activity, but also to provide additional characterization of the porous structure of different zeolites [36,37]. Here we have studied the catalytic cracking of two bulky alkylaromatics, di-isopropylbenzene (DIPB) and tri-isopropylbenzene (TIPB). DIPB (6.2 × 5.5 Å) is able to diffuse through 12-MR pores, whereas TIPB (9.5 × 5.5 Å) diffuses very slowly but will react with active sites located within extra-large pores, such as the 18-MR pores of ITQ-33, or on the external surface of the zeolite crystals.

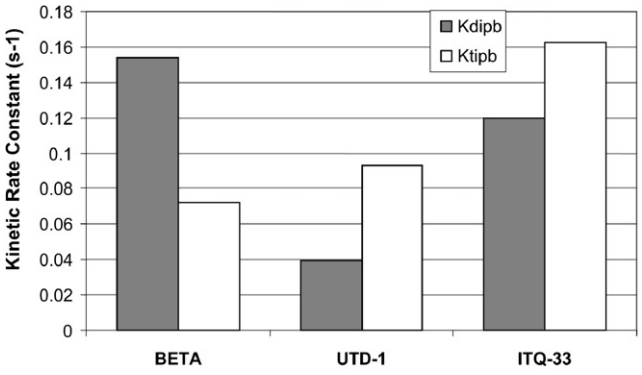

Fig. 9. First order kinetic rate constants for 1,3-di-isopropylbenzene and 1,3,5-tri-isopropylbenzene cracking over BETA, UTD-1 and ITQ-33.

Fig. 9 shows the first-order kinetic rate constants obtained for DIPB and TIPB cracking over Beta (12-MR pores), UTD-1 (14-MR pores), and ITQ-33 (18-MR pores). The figure demonstrates that the intrinsic activity as measured by cracking of 1,3-di-isopropylbenzene, which can diffuse in all of the zeolites studied, is higher for Beta and ITQ-33, due to their higher concentration of acid sites (Si/Al ratio = 30 and 20, respectively) compared with UTD-1 (Si/Al = 80). Comparing the activities per nominal Al site (Al/Al + Si) appears to show that the non-Ge zeolites (Beta and UTD-1) are more acidic due to their greater electronegativity [38].

However, in the case of the bulkier 1,3,5-tri-isopropylbenzene, UTD-1 with 14-MR pores gave a higher activity than Beta despite the much higher Si/Al ratio (Si/Al = 80) of the former. Finally, ITQ-33 with a T^{IV}/Al ratio of 20- and 18-MR pores gave the highest activity for the cracking of the bulkiest molecule. Interestingly, the cracking ratio TIPB/DIPB is larger for UTD-1 than for ITQ-33. This result cannot be explained solely by the affect of pore diameter. Indeed, if pore diameter were the only—or even the main—variable responsible for the results observed, then we would expect the TIPB/DIPB cracking ratio to be larger for ITQ-33. To explain our results, we can speculate that the shape of the pore (which is ellipsoidal in the case of UTD-1 instead of circular for ITQ-33) and/or the fact that some of the acid sites in ITQ-33 may indicate that the 10-MR channels may have a determining affect.

The effect of the larger pore size of zeolite ITQ-33 is also evidenced by the results obtained for benzene alkylation with propylene. Fig. 10 shows that ITQ-33 is not only very active, but also more resistant to deactivation than Beta zeolite.

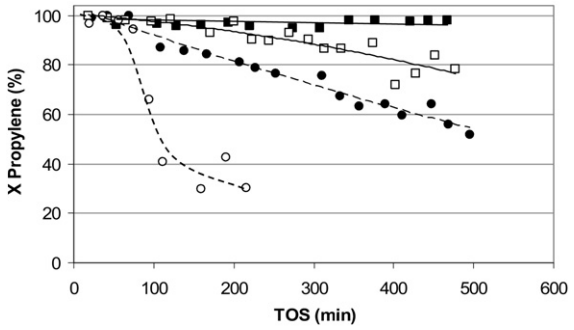

Fig. 10. Propylene conversion for zeolite ITQ-33 (squares) and BETA (circles) at 398 K, 3.5 MPa, benzene/propylene = 3.5 (mol/mol) and WHSV of 12 (black symbols) and 24 h^{-1} (open symbols).

Table 2
Alkylation of benzene with propylene using ITQ-33 and BETA zeolites. Product selectivity (wt%) at different space velocities WHSV = 12 and 24 h^{-1} at $T = 398$ K, $P = 3.5$ MPa, benzene/propylene = 3.5 mol mol^{-1}, TOS = 1 h

Catalyst	WHSV = 12 h^{-1}				WHSV = 24 h^{-1}			
	X	S_{cumene}	S_{DIPB}	S_{TIPB}	X	S_{cumene}	S_{DIPB}	S_{TIPB}
ITQ-33	98.6	76.5	17.3	3.7	98.7	63.8	23.0	7.8
BETA	95.7	90.0	6.9	<0.1	78.2	86.9	9.0	0.7

Catalyst deactivation occurs when alkylation is carried out in the presence of zeolites, due mainly to fouling or coking of the catalyst by propylene oligomerization products. Although commercial processes deal with this problem by combining reaction/regeneration cycles [39], there is a need to minimize olefin oligomerization and coking that increases catalyst life. The special microporous structure of ITQ-33 favors the formation and diffusion of the alkylation products while reducing the undesired propylene oligomerization. The benefits over the catalyst lifetime of this new zeolite compared with Beta are very clear, especially when space velocity is increased, as shown in Fig. 10. Besides its high stability, ITQ-33 is highly selective to alkylation products. The large 18-MR pores allow the formation of multialkylated products, such as di-isopropyl- and tri-isopropylbenzene, in larger proportions than with zeolite beta, as shown in Table 2. However, this is not detrimental, because most of the commercial cumene processes also include a transalkylation unit in which benzene is also fed and the multialkylated products can be reconverted to cumene [39,40]. Finally, a crucial issue that determines the suitability of a catalyst for production of cumene is its selectivity to *n*-propylbenzene, a highly undesired product formed by secondary intermolecular isomerization of cumene [41,42]. The selectivity to *n*-propylbenzene obtained in our experimental conditions was <100 ppm, a very good result compared with the specifications for commercial cumene processes, such as UOP Q-Max (250–300 ppm) [43] or ENI SpA (<500 ppm) [44].

4. Conclusions

An HT sequential experimental design allowed the synthesis of pure ITQ-33 zeolite that has a unique pore topology formed by 18-MR pores connected by 10-MR pores [26]. Despite its high Ge content, ITQ-33 remains stable provided that the organic is not removed. After calcination, it remains stable even in the presence of moisture at high temperatures. But if the zeolite is maintained in powder form at room temperature in presence of moisture, it rapidly loses crystallinity. The crystallinity loss is much slower in the zeolite in pelletized form. ITQ-33 shows medium-strong acidity, similar to that presented by 12-MR pore zeolites with the same chemical composition, indicating that larger pore diameter does not necessarily imply lower acid strength.

The benefits of the large pores and good acidity give ITQ-33 notable catalytic advantages for reacting bulkier molecules, as well as giving high activities and selectivities in the synthesis of cumene by alkylation of benzene with propylene.

Acknowledgments

The authors thank CICYT (MAT2003-07945-C02-01) for financial support. M.M. thanks CSIC for an I3P fellowship. The authors thank V. Clari for technical assistance and J. Martínez-Triguero for the cracking experiments on Beta and UTD-1.

References

[1] M.E. Davis, Nature 417 (2002) 813.
[2] A. Corma, J. Catal. 216 (2003) 298.
[3] P. Atienzar, M.J. Díaz-Cabañas, M. Moliner, E. Peris, A. Corma, H. García, Chem. Eur. J. 13 (2007) 8733.
[4] K.J. Balkus Jr., I. Bresinska, S. Kowalak, S.W. Young, Mater. Res. Soc. Symp. Ser. Proc. 223 (1991) 225.
[5] C.S. Cundy, P.A. Cox, Chem. Rev. 103 (2003) 663.
[6] A. Corma, M.E. Davis, Chem. Phys. Chem. 5 (2004) 304.
[7] A.W. Burton, J. Am. Chem. Soc. 129 (2007) 7627.
[8] G. Sastre, A. Pulido, R. Castaneda, A. Corma, J. Phys. Chem. B 108 (2004) 8830.
[9] S.I. Zones, S.-J. Hwang, S. Elomari, I. Ogino, M.E. Davis, A.W. Burton, C. R. Chim. 8 (2005) 267.
[10] K.G. Strohmaier, D.E.W. Vaughan, J. Am. Chem. Soc. 125 (2003) 16035.
[11] J.L. Paillaud, B. Harbuzaru, J. Patarin, N. Bats, Science 304 (2004) 990.
[12] G. Sastre, J.A. Vidal-Moya, T. Blasco, J. Rius, J.L. Jorda, M.T. Navarro, F. Rey, A. Corma, Angew. Chem. Int. Ed. 41 (2002) 4722.
[13] A. Corma, F. Rey, J. Rius, M.J. Sabater, S. Valencia, Nature 431 (2004) 287.
[14] A. Cantin, A. Corma, M.J. Diaz-Cabanas, J.L. Jorda, M. Moliner, J. Am. Chem. Soc. 128 (2006) 4216.
[15] R.F. Lobo, S.I. Zones, M.E. Davis, J. Incl. Phenom. 21 (1995) 47.
[16] R. Bialek, W.M. Meier, M. Davis, M.J. Annen, Zeolites 11 (1991) 438.
[17] S.I. Zones, M.M. Olmstead, D.S. Santilli, J. Am. Chem. Soc. 114 (1992) 4195.
[18] R.F. Lobo, M. Pan, I. Chan, H.X. Li, R.C. Medrud, S.I. Zones, P.A. Crozier, M.E. Davis, Science 262 (1993) 1543.
[19] R.F. Lobo, M.E. Davis, J. Am. Chem. Soc. 117 (1995) 3766.
[20] Y. Mathieu, J.-L. Paillaud, P. Caullet, N. Bats, Micropor. Mesopor. Mater. 75 (2004) 13.
[21] N. Bats, L. Rouleau, J.L. Paillaud, P. Caullet, Y. Mathieu, S. Lacombe, Stud. Surf. Sci. Catal. 154A (2004) 283.
[22] A. Corma, M. Puche, F. Rey, G. Sankar, S.J. Teat, Angew. Chem. Int. Ed. 42 (2003) 2702.
[23] T. Boix, M. Puche, M.A. Camblor, A. Corma, U.S. patent 6471941, 2002.
[24] A. Corma, F. Rey, S. Valencia, J.L. Jorda, J. Rius, Nat. Mater. 2 (2003) 493.
[25] R. Castañeda, A. Corma, V. Fornes, F. Rey, J. Rius, J. Am. Chem. Soc. 125 (2003) 7820.

[26] A. Corma, M.J. Diaz-Cabanas, J.L. Jorda, C. Martinez, M. Moliner, Nature 443 (2006) 842.
[27] A. Corma, M. Moliner, J.M. Serra, P. Serna, M.J. Diaz-Cabanas, L. Baumes, Chem. Mater. 18 (2006) 3287.
[28] A. Corma, M.J. Diaz-Cabanas, M. Moliner, C. Martinez, J. Catal. 241 (2006) 312.
[29] M. Moliner, J.M. Serra, A. Corma, E. Argente, S. Valero, V. Botti, Micropor. Mesopor. Mater. 78 (2005) 73.
[30] R.F. Lobo, M. Tsapatsis, C.C. Freyhardt, I. Chan, C.-Y. Chen, S.I. Zones, M.E. Davis, J. Am. Chem. Soc. 119 (1997) 3732.
[31] J.P. Guth, H. Kessler, P. Caullet, J. Hazm, J. Merrouche, J. Patarin, in: Proc. 9th Int. Zeolite Conf., vol. 1, 1993, p. 215.
[32] H. Kosslick, V.A. Tuan, R. Fricke, Ch. Peuker, W. Pilz, W. Storek, J. Phys. Chem. 97 (1993) 5678.
[33] S. Leiva, M.J. Sabater, S. Valencia, G. Sastre, V. Fornes, F. Rey, A. Corma, C. R. Chim. 8 (2005) 369.
[34] D. Barthomeuf, J. Chem. Soc. Chem. Commun. (1977) 743.
[35] F. Eder, M. Stockenhuber, J.A. Lercher, J. Phys. Chem. B 101 (1997) 5414.
[36] A. Corma, V. Fornés, L. Forni, F. Márquez, J. Martínez-Triguero, D. Moscotti, J. Catal. 179 (1998) 451.
[37] J. Martinez-Triguero, M.J. Diaz-Cabanas, M.A. Camblor, V. Fornes, T.L.M. Maesen, A. Corma, J. Catal. 182 (1999) 463.
[38] W.J. Mortier, J. Catal. 55 (1978) 138.
[39] T.F. Degnan Jr., C.M. Smith, C.R. Venka, Appl. Catal. A Gen. 221 (2001) 283.
[40] C. Perego, P. Ingallina, Catal. Today 73 (2002) 3.
[41] J. Cejka, B. Wichterlova, Catal. Rev. Sci. Eng. 44 (3) (2002) 375.
[42] E.G. Derouane, H. He, S.B.D.A. Hamid, I.I. Ivanova, Catal. Lett. 58 (1) (1999) 1.
[43] http://www.uop.com/objects/31%20Q_MAX.pdf.
[44] http://www.polimerieuropa.com/it/pdf/cumene.pdf.